CrossMark
click for updates

# Improved stability of amorphous zinc tin oxide thin film transistors using molecular passivation

M. S. Rajachidambaram,[1] A. Pandey,[2] S. Vilayurganapathy,[2] P. Nachimuthu,[2] S. Thevuthasan,[2] and G. S. Herman[1,a]

[1]School of Chemical, Biological, and Environmental Engineering, Oregon State University, Corvallis, Oregon 97331, USA
[2]Environmental Molecular Sciences Laboratory, Pacific Northwest National Laboratory, Richland, Washington 99354, USA

The role of back channel surface chemistry on amorphous zinc tin oxide (ZTO) bottom gate thin film transistors (TFTs) has been characterized by positive bias-stress measurements and x-ray photoelectron spectroscopy. Positive bias-stress turn-on voltage shifts for ZTO-TFTs were significantly reduced by passivation of back channel surfaces with self-assembled monolayers of n-hexylphosphonic acid when compared to ZTO-TFTs with no passivation. These results indicate that adsorption of molecular species on the exposed back channel of ZTO-TFTs strongly influence observed turn-on voltage shifts, as opposed to charge injection into the dielectric or trapping due to oxygen vacancies. © 2013 AIP Publishing LLC. [http://dx.doi.org/10.1063/1.4826457]

Transparent amorphous oxide semiconductors (TAOS), including indium gallium zinc oxide (IGZO) and zinc tin oxide (ZTO), are of considerable interest as active channel materials for thin film transistors (TFTs).[1,2] TAOS-TFTs have relatively high average electron mobilities ($\mu_{avg} > 10$ cm$^2$/Vs), despite being amorphous, and have been integrated into active-matrix liquid crystal displays (AM-LCD) and active-matrix organic light emitting diode displays (AM-OLED).[3,4] TAOS-TFTs may eventually replace amorphous silicon TFT technologies for these and many other applications.[5] An important requirement for display applications is high electrical stability, since bias, current, and/or light induced instabilities may cause non-uniformities by changing the relative brightness of individual pixels. Bias stress stability of TAOS-TFTs has been intensely investigated for both ZTO and IGZO, where effects of composition, process temperature, process method, gate dielectric, back channel passivation, and other factors have been evaluated.[6–13] Proposed mechanisms for positive bias stress threshold voltage shifts for TAOS-TFTs include electron trapping at the semiconductor/dielectric interface, electron injection into the dielectric, or formation of sub-band gap states in the bulk of films. It has also been suggested that dense passivation layers are necessary to minimize threshold voltage shifts for TAOS-TFTs.[3–5]

Recent studies indicated that threshold voltage shifts for TAOS-TFTs could be strongly influenced by adsorption/desorption of molecules (e.g., O$_2$ and H$_2$O) on exposed back channel surfaces.[8,12,14–16] Chemisorption of molecules with oxide semiconductors has been well studied especially in regard to the role of charge transfer during chemisorption and the corresponding effect on conductivity for gas sensors.[17,18] For oxide semiconductors, adsorbed molecular oxygen can accept electrons from the surface resulting in formation of a depletion layer, while absorbed water can donate electrons to the surface resulting in formation of an accumulation layer.[15,16] Both processes significantly change electron density at the back channel surface and can shift the threshold voltage, where a depletion layer gives a positive threshold voltage shift, whereas an accumulation layer gives a negative threshold voltage shift.[8,14,19] Recently positive shifts in threshold voltage were used to monitor adsorption of molecular oxygen on a ZTO-TFT for sensing applications.[17] For most TFT applications, it is desirable to minimize back channel interactions and their effect on device stability, and that is why a variety of passivation layers are currently being used.[3–5]

In this letter, we demonstrate the use of n-hexylphosphonic acid (n-HPA) self-assembled monolayers (SAM) as molecular passivation layers for ZTO-TFT back channel surfaces. ZTO surface chemistries were characterized using contact angle measurements, positive bias stress turn-on voltage shifts, and x-ray photoelectron spectroscopy (XPS). Significant improvements in ZTO-TFT turn-on voltage stabilities were observed for n-HPA passivated surfaces and these results provide a means to better understand the role of defect passivation at back channel surfaces of TAOS materials.

Heavily p-doped Si substrates were used as the gate electrode, where a thermally grown SiO$_2$ (100 nm) layer was used as the gate dielectric. Substrates were cleaned prior to TFT fabrication with acetone, isopropyl alcohol (IPA), DI water, and a UV-Ozone treatment for 1 h. Amorphous ZTO films were deposited by RF magnetron sputter deposition ($\sim$40 nm thick) using a 3 in. ZTO target (2:1 ZnO:SnO$_2$), 100 W RF power, $\sim$4 mTorr chamber pressure, and 20 sccm flow rate with a 1:19 (O$_2$:Ar) ratio. Active layers were patterned using a shadow mask during ZTO deposition. ZTO films were annealed to 600 °C in air, for optimal device performance.[20] Source and drain layers were patterned using a shadow mask during thermal evaporation of Al ($\sim$500 nm thick) resulting in a W/L ratio of 1000 $\mu$m/200 $\mu$m. Back channel surface passivation was performed by UV-Ozone treatment for 1 h followed by immediate immersion of the samples in 2 mM n-HPA solution in 95% ethanol. Samples were removed from solution, rinsed with 95% ethanol, and dried with flowing nitrogen. The

[a]Author to whom correspondence should be addressed. Electronic mail: greg.herman@oregonstate.edu
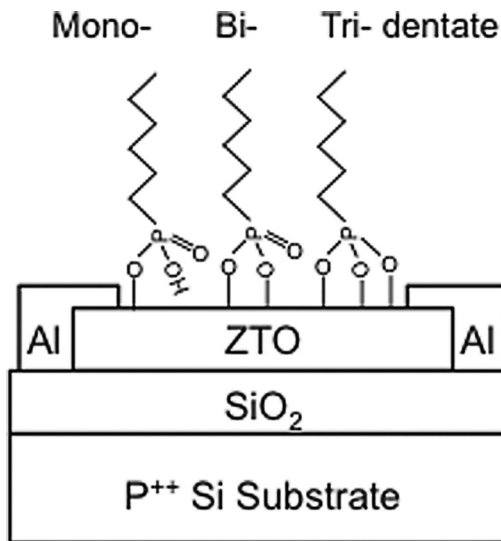
FIG. 1. Schematic illustration of n-HPA functionalized ZTO TFT structure showing the mono-, bi-, and tri-dentate binding of n-HPA to ZTO.

water contact angle increased for increasing soak times due to adsorption of n-HPA, and reduction in surface energy due to alkane groups. The highest contact angle (104.8°) was obtained after a 16 h soak, and this time was used for the experiments in this study. The n-HPA passivated ZTO-TFTs were either characterized with no further treatment, or after a post-anneal at 140 °C for 48 h in flowing dry nitrogen for n-HPA bond activation.[21] After the post-anneal, samples were sonicated in a 5% triethylamine/ethanol solution, rinsed with 95% ethanol, and dried with flowing nitrogen. Duplicate ZTO-TFTs were fabricated where they have gone through identical processing steps as passivated samples, other than a n-HPA soak. A schematic of the device structure is shown in Figure 1, as well as possible bonding of n-HPA to the ZTO surface. All TFT bias-stress measurements were performed in a dark box at room temperature in air using an Agilent 4155C precision semiconductor parameter analyzer. Single sweep source-to-drain current versus gate voltage ($I_{DS}$-$V_{GS}$) transfer curves were measured with the drain voltage ($V_{DS}$) set to 1 V. Stress measurements were performed up to $10^4$ s using an applied $V_{GS}$ of 10 V (1 MV/cm) and $V_{DS}$ set to 0 V. XPS data were fit using XPSPEAK 4.1, where the most intense peak in the spectrum defined the full-width-half-maximum (FWHM) and Gaussian-Lorentzian mixing for a given core-level. A linear background was used to fit all spectra. To minimize complications due to sample charging or band bending, the binding energy scale was referenced to the C 1s spectra, which was set to 284.6 eV.

In Figures 2(a) and 2(b) we show positive bias stress $I_{DS}$-$V_{GS}$ data for ZTO-TFTs without and with an n-HPA passivation layer (devices with no post anneal) and for bias stress times of 0, 10, 100, 1000, and 10 000 s. The arrows indicate the direction of turn on voltage shift ($\Delta V_{ON}$) for increasing bias stress time. In Table I, we provide the average mobility ($\mu_{avg}$), $V_{ON}$, and drain current on-to-off ratio ($I_{ON}/I_{OFF}$) for unstressed devices. These parameters were extracted using methods described previously.[22] It was observed that as the duration of bias stress increased the $I_{DS}$-$V_{GS}$ data had a positive turn-on voltage shift for all samples, and that both

sub-threshold slope and $\mu_{avg}$ remained unchanged. In Figure 2(c), we plot $\Delta V_{ON}$ versus bias stress time for all four ZTO-TFTs. Devices without n-HPA passivation had the largest bias stress $\Delta V_{ON}$, where RT (open circles) and 140 °C post-annealed (open squares) devices had shifts of 0.8 and 1.5 V after 10 000 s, respectively. For bias stress induced trapping and metastability, a stretched exponential model has been previously employed for amorphous silicon-[23] and ZTO-TFTs[11,13,24,25]
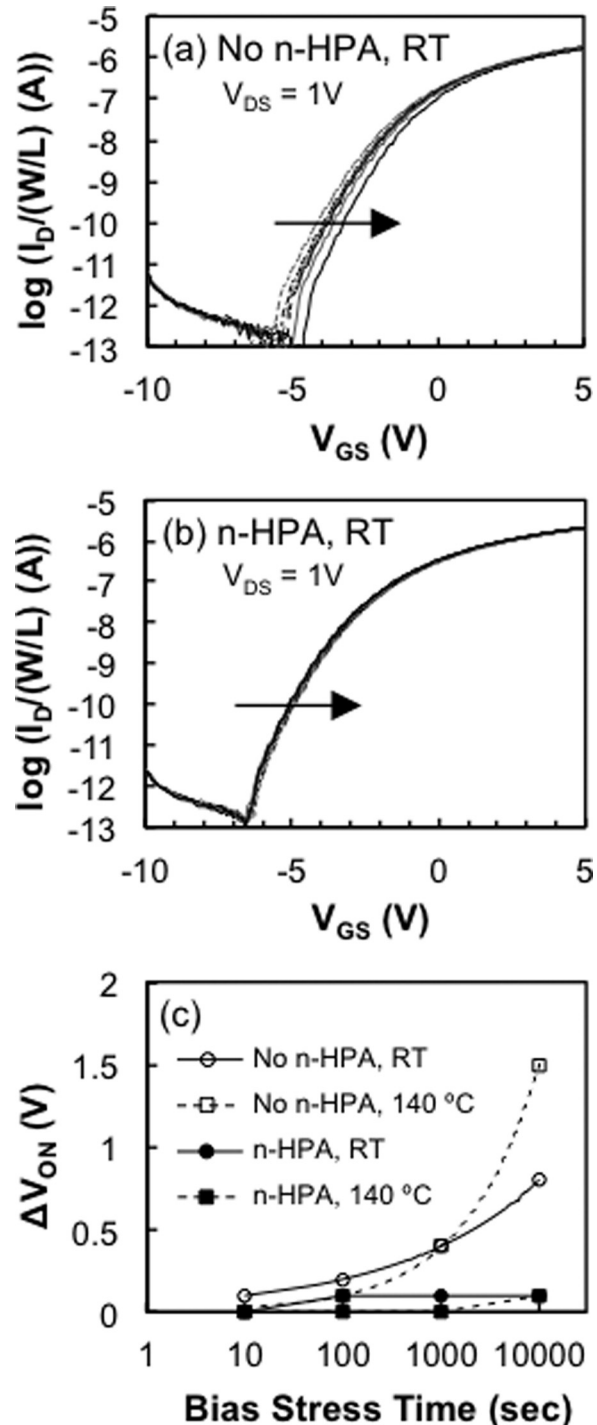


FIG. 2. Plot of $I_D$ vs $V_{GS}$ for various treatments of the ZTO TFTs as a function of positive biased stress time. (a) Without n-HPA, no post-annealed, (b) with n-HPA, no post-annealed. (c) $\Delta V_{ON}$ shift vs positive bias stress time (s) for ZTO TFTs with/without n-HPA and with/without post-annealing. For devices without n-HPA, a fit of the stretched exponential model (solid and dashed lines) is shown.

TABLE I. Average mobility and turn on voltage for ZTO TFTs with/without n-HPA and with/without post-annealing.

| ZTO-TFT | $\mu_{ave}$ (cm$^2$/Vs) | $V_{on}$ (V) | $I_{ON}/I_{OFF}$ |
|---|---|---|---|
| No n-HPA, RT | 12.0 | −5.1 | $1.4 \times 10^6$ |
| n-HPA, RT | 10.7 | −6.0 | $2.8 \times 10^6$ |
| No n-HPA, 140 °C | 12.5 | −12.8 | $3.5 \times 10^6$ |
| n-HPA, 140 °C | 12.3 | −4.7 | $3.3 \times 10^6$ |

$$\Delta V_{th} = \Delta V_o \left\{ 1 - \exp\left[ -\left(\frac{t}{\tau}\right)^\beta \right] \right\}, \qquad (1)$$

where the effective voltage drop across the gate oxide ($\Delta V_o$) is approximately given by the difference between gate stress voltage and initial threshold voltage ($V_{G,stress} - V_{th,i}$), and characteristic trapping time of carriers ($\tau$), and stretched exponential exponent ($\beta$), both of which are dependent on stress bias. For our studies we used $V_{ON}$ in place of $V_{th}$, where $V_{ON}$ was obtained by extrapolation from log $I_D$ versus $V_{GS}$ plots where log ($I_D/(W/L)$) (A) is equal to −11. This procedure allowed us to determine bias induced shifts with higher precision than $V_{th}$, although the magnitude of shifts by either approach was nearly equivalent.

As shown in Figure 2(c), excellent fits to positive bias stress $V_{ON}$ shifts were obtained by the stretched exponential model for ZTO devices without n-HPA passivation, and RT (solid line) and 140 °C (dashed line) post-annealing treatments. Extracted values of $\tau$ and $\beta$ for different thermal treatments are summarized in Table II, and were in good agreement with literature values. For example, characteristic trapping times for amorphous Si TFTs with a SiN$_x$ gate insulator was $\sim 10^8$ s,[18] for RF-sputter deposited ZTO with a PECVD SiO$_2$ gate insulator was $\sim 3.9 \times 10^5$ s,[6] and for an ink-jet printed ZTO TFTs with a PECVD SiO$_2$ gate insulator was $\sim 6.0 \times 10^4$ s.[21] The stretched exponential model is primarily used to describe $V_{ON}$ shifts due to trapping at the dielectric interface or due to metastability in the channel material, although as discussed below this model can also be used to describe $V_{ON}$ shifts due to back channel chemical effects. As shown in Figure 2(c), no positive bias stress $V_{ON}$ shifts were observed for ZTO devices with n-HPA passivation, and RT (solid line) and 140 °C (dashed line) post-annealing treatments. Since devices with and without n-HPA passivation had identical preparation of dielectric/ZTO interfaces and ZTO post deposition annealing conditions, the positive bias stress $V_{ON}$ shifts were most likely due to chemistry at the back channel interface as opposed to trapping at the dielectric interface or due to metastability in the channel material.

In the lower portion of Figure 3, we show O 1s XPS data for a blanket ZTO film after being annealed to 600 °C

TABLE II. Characteristic trapping time of carriers, $\tau$ and stretched exponential exponent, $\beta$ for ZTO TFTs (without n-HPA) with/without post-annealing.

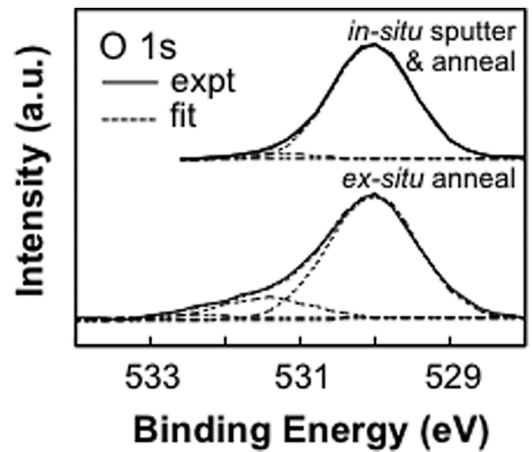| ZTO–no n-HPA–post annealing conditions | $\tau$ (s) | $\beta$ |
|---|---|---|
| RT | $1.4 \times 10^8$ | 0.30 |
| 140 °C | $9.0 \times 10^5$ | 0.59 |



FIG. 3. O 1s XPS data obtained from blanket ZTO films that have been annealed to 600 °C for 60 min in air (*ex-situ* anneal) and the same sample after being annealed to 550 °C for 15 min in P(O$_2$) = 1 × 10$^{-6}$ Torr (*in-situ* anneal) without exposure to ambient atmosphere.

for 60 min in air (*ex-situ* anneal). To minimize surface contamination the sample was introduced into the vacuum system prior to cooling below 100 °C. It was necessary to fit the O 1s core level spectrum for *ex-situ* annealed ZTO samples with three components, similar to what has been done previously for ZTO and related materials.[11,18,26,27] We have determined that the binding energies for the three components were at 530.4, 531.7, and 532.9 eV. For several prior ZTO XPS studies,[9,11,24,28] the O 1s peak components were assigned as follows. The low-energy peak corresponds to lattice oxygen ions, which have neighboring Zn and Sn ions. The mid-energy peak corresponds to lattice oxygen in oxygen-deficient regions. The high-energy peak corresponds to a surface hydroxide or oxyhydroxide species. It was also proposed that the intensity of the mid-energy peak could be correlated with the number of oxygen vacancies in the ZTO and the corresponding number of traps, which influence the bias stress stability of devices fabricated from TAOS materials.[11] Similar peak assignments have been made for other amorphous oxide semiconductors.[29–31] For two other ZTO XPS studies,[18,25] the O 1s peak components were assigned as follows. The low-energy peak corresponds to lattice oxygen ions, which have neighboring Zn and Sn ions (same as above). The mid-energy peak corresponds to surface hydroxyl species. The high-energy peak corresponds to surface water or carbonate species. The mid-energy peak in this case could be correlated with the number of adsorbed species on the ZTO surface and the corresponding number of adsorbate-induced traps, which influence the bias stress stability of devices fabricated from TAOS materials

To determine the origin of the three O 1s components we have performed *in-situ* annealing experiments to either remove adsorbed species from the ZTO surface or increase the number of oxygen vacancies in the ZTO film. In the upper portion of Figure 3 we show O 1s XPS data for the *ex-situ* annealed sample after heating to 550 °C for 15 min in P(O$_2$) = 1 × 10$^{-6}$ Torr (*in-situ* anneal) without exposure to ambient atmosphere. We found that only two components were necessary to fit the O 1s core level spectrum for the *in-situ* annealed ZTO sample, where the components

correspond to the low-energy (530.4 eV) and mid-energy (531.7 eV) peak positions, similar to the *ex-situ* annealed sample. These components correspond to lattice oxygen ions, which have neighboring Zn and Sn ions, and either lattice oxygen in oxygen-deficient regions or surface hydroxyl species. Since the *in-situ* annealing experiments were performed in an oxygen deficient atmosphere compared with the *ex-situ* annealing experiments, it would be expected that the number of oxygen vacancies would increase for the former, resulting in an increased intensity for the mid-energy O 1s component. However, we find that the mid-energy O 1s component was significantly reduced in intensity, while the high-energy O 1s component was completely eliminated by *in-situ* annealing. These results suggest that the mid- and high-energy O 1s components were due to adsorbed species, and not oxygen deficient regions in the material. Thus, the mid-energy peak intensity should be correlated with the number of adsorbed species on the ZTO back surface (i.e., not the number of oxygen vacancies in the ZTO and the corresponding number of traps), and it was these adsorbed species that influence the bias stress stability of the devices.

In Figure 4 we show high-resolution O 1s XPS data, which were obtained directly from the devices measured in Figure 2. These data were obtained to investigate changes in ZTO TFT back channel chemistry depending on sample preparation (i.e., with/without n-HPA, and with/without a post-annealing step). As above, the O1s spectra for ZTO devices with no n-HPA required three components to obtain an adequately fit. These spectra and the corresponding fits are shown in the lower portion of Figure 4. For the O 1s spectra for ZTO devices with n-HPA we required three components to obtain an adequate fit. These spectra and the corresponding fits are shown in the upper portion of Figure 4. The low-energy peak corresponds to lattice oxygen ions,
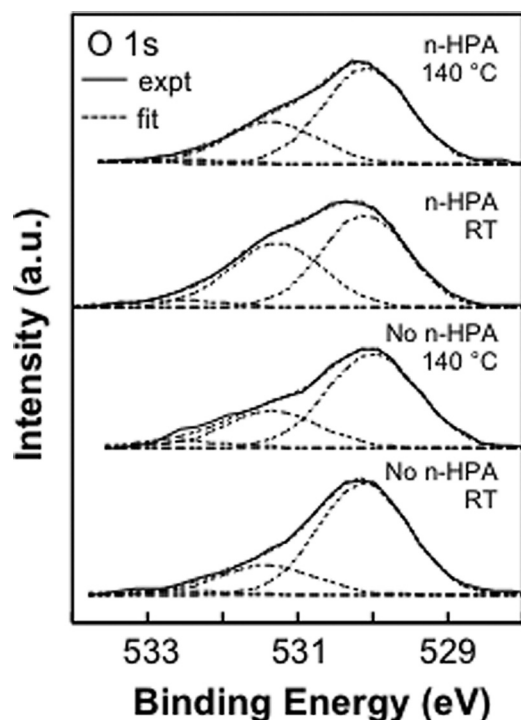
which have neighboring Zn and Sn ions (same as above). The mid-energy O 1s components could be attributed to P-O-Zn/P-O-Sn and P=O, which was consistent with prior studies.[19,32] The third peak at a higher binding energy of 532.5 eV could be assigned to P-OH species.[19,26]

These results strongly suggest that the back channel surface chemistry was the dominant reason for bias-stress turn-on voltage shifts for these ZTO TFTs. There are several mechanisms that have been proposed to describe device instabilities due to the back channel surface chemistry, including field-induced adsorption/desorption,[8] dipole interactions,[33] and charge transfer.[15,16] Recent studies suggested that water adsorption was the dominant species for ZTO TFT instabilities leading to significant shifts in threshold voltage,[15] and increased hysteresis in the ZTO TFT transfer characteristics (difference in the up and down sweeps in the $I_{DS}$-$V_{GS}$ data).[16] The saturation coverage of n-HPA used in these studies significantly limits the interaction of impurity species, especially $H_2O$, with the ZTO surface. For example, n-HPA has previously been shown to be effective as an etch protection layer for ZnO,[32] and as a protection layer from atmospheric contaminants for indium tin oxide.[34] Based on the results from this study we propose that n-HPA is an effective barrier that limits the interaction of water with the ZTO surface, and that n-HPA does not provide electron trap and/or donor states that would result in device instabilities. Finally, we have not observed significant differences in the ZTO TFT hysteresis for the different surface treatments, which suggests that n-HPA does not degrade device performance.

In summary, highly stable ZTO TFTs were fabricated through molecular passivation of the ZTO back channel surface. Bias stress dependence of the turn-on voltage shifts for unpassivated ZTO TFTs was best described by a stretched exponential model, whereas n-HPA passivated ZTO TFTs essentially had no turn-on voltage shifts for the same bias stress conditions. Bias stress measurements and XPS analysis suggest that reductions in the turn-on voltage shifts were related to improved TFT stability due to well defined molecular passivation at the backchannel surface, which limits electrical modification of the channel due to the adsorption of impurity species (i.e., $O_2$, $H_2O$, etc.). This is in contrast to models that propose oxygen vacancy suppression based on changes observed in the O 1s spectra for different process treatments or chemical compositions. Finally, we propose that these molecular passivation layers limit ambient $H_2O$ interactions with the ZTO back channel surface and thus prevent $H_2O$ from providing electron trap and/or donor states.

FIG. 4. O 1s XPS data obtained from ZTO TFTs with/without n-HPA and with/without post-annealing.

[1] K. Nomura, H. Ohta, A. Takagi, T. Kamiya, M. Hirano, and H. Hosonon, Nature **432**, 488 (2004).

[2] H. Q. Chiang, J. F. Wager, R. L. Hoffman, J. Jeong, and D. A. Keszler, Appl. Phys. Lett. **86**, 013503 (2005).

[3] T. Kamiya, K. Nomura, and H. Hosono, Sci. Technol. Adv. Mater. **11**, 044305 (2010).

[4] E. Fortunato, P. Barquinha, and R. Martins, Adv. Mater. **24**, 2945 (2012).

[5] J. F. Wager, D. A. Keszler, and R. E. Presley, *Transparent Electronics* (Springer, New York, 2008).

[6] P. Görrn, P. Hölzer, T. Riedl, W. Kowalsky, J. Wang, T. Weimann, P. Hinze, and S. Kipp, Appl. Phys. Lett. **90**, 063502 (2007).

[7] A. Suresh and J. F. Muth, Appl. Phys. Lett. **92**, 033502 (2008).

[8] J. K. Jeong, H. W. Yang, J. H. Jeong, Y.-G. Mo, and H. D. Kim, Appl. Phys. Lett. **93**, 123508 (2008).

[9] S. Yang, K. H. Ji, U. K. Kim, C. S. Hwang, S.-H. K. Park, C.-S. Hwang, J. Jang, and J. K. Jeong, Appl. Phys. Lett. **99**, 102103 (2011).

[10] M. Fakhri, P. Görrm, T. Weimann, P. Hinze, and T. Riedl, Appl. Phys. Lett. **99**, 123503 (2011).

[11] S.-J. Seo, J. H. Jeon, Y. H. Hwang, and B.-S. Bae, Appl. Phys. Lett. **99**, 152102 (2011).

[12] P. Görrn, T. Riedl, and W. Kowalsky, J. Phys. Chem. C **113**, 11126 (2009).

[13] W. B. Jackson, R. Hoffman, B. Yeh, T. Emery, T. Koch, C. McConica, and O. Kwon, Phys. Status Solidi A **207**, 695 (2010).

[14] S.-Y. Sung, J. H. Choi, U. B. Han, K. C. Lee, J.-H. Lee, J.-J. Kim, W. Lim, S. J. Pearton, D. P. Norton, and Y.-W. Heo, Appl. Phys. Lett. **96**, 102107 (2010).

[15] D. Kim, S. Yoon, Y. Jeong, Y. Kim, and M. Hong, Appl. Phys. Express **5**, 021101 (2012).

[16] M. Fakhri, H. Johann, P. Görrn, and T. Riedl, ACS Appl. Mater. Interfaces **4**, 4453 (2012).

[17] W. Göpel, Prog. Surf. Sci. **20**, 9 (1985).

[18] M. Batzill and U. Diebold, Prog. Surf. Sci. **79**, 47 (2005).

[19] Y.-C. Chen, T.-C. Chang, H.-W. Li, W.-F. Chung, C.-P. Wu, S.-C. Chen, J. Lu, Y.-H. Chen, and Y.-H. Tai, Appl. Phys. Lett. **100**, 262908 (2012).

[20] J. S. Rajachidambaram, S. Sanhavi, P. Nachimuthu, V. Shutthanandan, T. Varga, B. Flynn, S. Thevuthasan, and G. S. Herman, J. Mater. Res. **27**, 2309 (2012).

[21] P. J. Hotchkiss, M. Malicki, A. J. Giordano, N. R. Armstrong, and S. R. Mader, J. Mater. Chem. **21**, 3107 (2011).

[22] R. L. Hoffman, J. Appl. Phys. **95**, 5813 (2004).

[23] F. R. Libsch and J. Kanicki, Appl. Phys. Lett. **62**, 1286 (1993).

[24] J. Triska, J. F. Conley, R. Presley, and J. F. Wager, J. Vac. Sci. Technol. B **28**(4), C5I1 (2010).

[25] C. Avis and J. Jang, Electrochem. Solid-State Lett. **14**, J9 (2011).

[26] M. G. Kim, H. S. Kim, Y. G. Ha, J. He, M. G. Kanatzidis, A. Facchetti, and T. J. Marks, J. Am. Chem. Soc. **132**, 10352 (2010).

[27] M.-G. Kim, M. G. Kanatzidis, A. Facchetti, and T. J. Marks, Nature Mater. **10**, 382 (2011).

[28] P. K. Nayak, M. N. Hedhili, D. Cha, and H. N. Alshareef, ACS Appl. Mater. Interfaces **5**, 3587 (2013).

[29] B. S. Yang, M. S. Huh, S. Oh, U. S. Lee, Y. J. Kim, M. S. Oh, J. K. Jeong, C. S. Hwang, and H. J. Kim, Appl. Phys. Lett. **98**, 122110 (2011).

[30] P. Carreras, S. Gutmann, A. Antony, J. Bertomeu, and R. Schlaf, J. Appl. Phys. **110**, 073711 (2011).

[31] Y.-C. Huang, P.-Y. Yang, H.-Y. Huang, S.-J. Wang, and H.-C. Cheng, J. Nanosci. Nanotechnol. **12**, 5625 (2012).

[32] C. L. Perkins, J. Phys. Chem. C **113**, 18276 (2009).

[33] Y.-H. Kim, H. S. Kim, J.-I. Han, and S. K. Park, Appl. Phys. Lett. **97**, 092105 (2010).

[34] S. A. Paniagua, P. J. Hotchkiss, S. C. Jones, S. R. Marder, A. Mudalige, F. S. Marrikar, J. E. Pemberton, and N. R. Armstrong, J. Phys. Chem. C **112**, 7809 (2008).